Laser calibration of an impact disdrometer

John E. Lane
Easi-ESC, Kennedy Space Center, FL, USA
John.E.Lane@nasa.gov

Takis Kasparis
Cyprus University of Technology, Lemesos, Cyprus
Takis.Kasparis@cut.ac.cy

Philip T. Metzger
NASA, Kennedy Space Center, FL, USA
Philip.T.Metzger@nasa.gov

W. Linwood Jones
University of Central Florida, Orlando, FL, USA
ljones@ucf.edu

Abstract: A practical approach to developing an operational low-cost disdrometer hinges on implementing an effective in situ adaptive calibration strategy. This calibration strategy lowers the cost of the device and provides a method to guarantee continued automatic calibration. In previous work, a collocated tipping bucket rain gauge was utilized to provide a calibration signal to the disdrometer's digital signal processing software. Rainfall rate is proportional to the 11/3 moment of the drop size distribution (a 7/2 moment can also be assumed, depending on the choice of terminal velocity relationship). In the previous case, the disdrometer calibration was characterized and weighted to the 11/3 moment of the drop size distribution (DSD). Optical extinction by rainfall is proportional to the 2^{nd} moment of the DSD. Using visible laser light as a means to focus and generate an auxiliary calibration signal, the adaptive calibration processing is significantly improved.

1. Introduction

An impact rainfall disdrometer developed at the University of Central Florida, Department of Electrical and Computer Engineering, in conjunction with Cyprus University of Technology, has been in operation on the roof of the Engineering Building at the main campus in Orlando since 2009. The instrument utilizes low-cost piezoelectric transducers configured in a dual head arrangement, allowing the total desired sensing area of 50 cm^2 (area of Joss disdrometer) to be distributed uniformially over the cross-section of standard off-the-shelf piezoelectric disks. The disdrometer audio output from the piezos are summed with a gated sine wave oscillator, triggered by a collocated tipping bucket's switch closure. When the tipping bucket tips, after every accumulation of 0.01 inch rainfall, a short burst of the characteristic sine wave is injected into the audio signal. This provides tipping bucket data on a single audio channel with the disdrometer data. Multiple tipping buckets can be connected to the same line using oscillators of different frequencies. The identity of the tipping bucket can be decoded using the Goertzel algorithm during the signal processing phase. The *Dual-Head Disdrometer* (DHD) has been successfully collecting data for more than three years. The drop size distributions (DSD) measured by the DHD are compared to other collocated instruments.

The first benefit from a collocated laser extinction measurement is to provide additional data not previously available for disdrometer in situ calibration. In situ calibration of disdrometers is not a commonly used technique, but previous research (Kasparis, 2010) demonstrates that it can be one of the best strategies leading towards implementation and deployment of lower cost disdrometers. Lower cost disdrometers then translates into more disdrometers per research project to study spatial and temporal variability of the rainfall DSD. Another benefit of using direct measurement of the DSD's second moment is to provide additional data to a 3D-DSD model (Lane, 2009). An ideal description of rainfall is in terms of its DSD, as a function of x, y, z, and t: $N(D;x,y,z,t)$. In this sense, the 3D-DSD uses all available data, including NEXRAD, rain gauges, disdrometers, optical extinction, and wind data.

2. DHD Fabrication

During a 2009-2010 joint project between CUT and UCF, numerous iterations of potential low-cost disdrometer prototypes were fabricated and tested. Design goals included use of COTS piezoelectric buzzer disks of various sizes and in various combinations, with an electrically isolating, moisture barrier encapsulating material. In all iterations, the total sensing area was limited to a range of 50 to 100 cm^2. For reference, the Joss disdrometer sensor area is 50 cm^2. The size options of COTS piezoelectric disks are limited to a few standard diameters. The largest diameter that was found as a COTS component is the muRata 7NB-41-1 piezoelectric diaphragm. The component dimensions of the 7NB-41-1 are shown in Figure 2. The ceramic diameter is 25 mm and nickel alloy substrate is 41 mm in diameter.

The goal of the encapsulating material is to provide a moisture seal, but an equally important purpose is to provide mass loading and damping to the ceramic disk. Various encapsulating materials were used from a hard marine epoxy with a Shore D hardness of 72 to a soft Cytec Conathane EN-12 polyurethane with a Shore A hardness of 50. Many of the configurations tested consisted of an additional thin plastic cover, with a milled angled slope to encourage water roll off. Figure 3 shows two multi-ceramic configurations with a total sensor area (outside diameter of encapsulate) equal to 65 cm^2. Figure 4 shows the final dual-head configuration, with a total area of 58.4 cm^2.

During fabrication, one of the biggest challenges was to eliminate or at least minimize the number of bubbles that formed in the epoxy as it cured. No good method was found, even though it was suggested that pulling a partial vacuum around the mold may reduce the number of bubbles. In the end, there was no easy solution to the formation of bubbles. It appeared that fewer bubbles formed in the hard epoxy than in the soft urethane.

3. SDOF Model of Impact Sensor

An impact disdrometer can be roughly modeled as a single degree of freedom (SDOF) system. Some disdrometer designs are better approximated by an SDOF system than others. The goal of the model is to provide some insight into the sensor response, which then helps guide the signal processing design.

*** The following will be converted to Word, but for purposes of the DAA review draft, it will remain as a PowerPoint insert (the conversion will be a format change only):

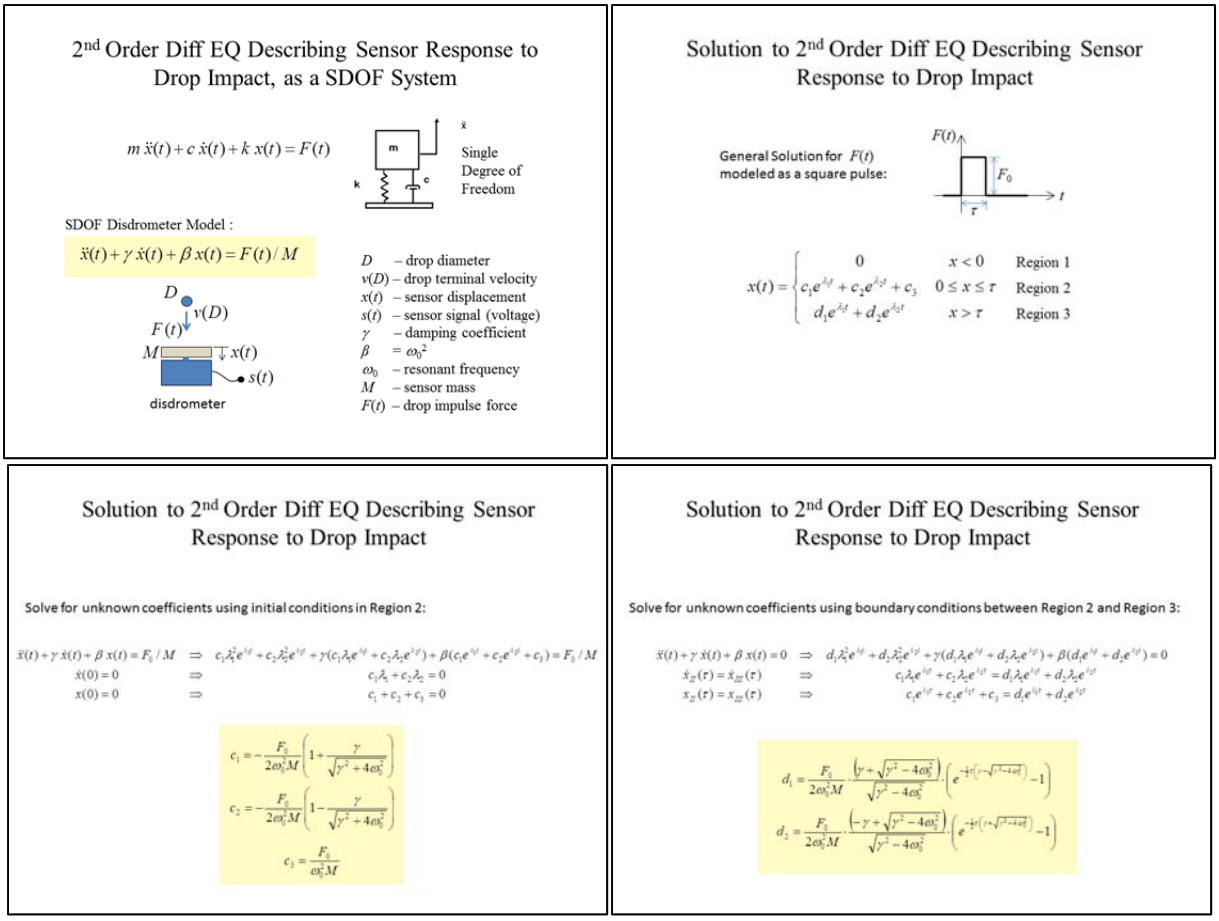

Figure 5 shows a typical DOF response output with a square pulse input, corresponding to an approximation of a drop impulse. The SDOF predictions are very similar to the electrical signal shapes seen in most of these designs. The log plot to the right in Figure 5 demonstrates that there is little difference in the peak amplitude or the area under the curve as a means to back out the drop size from the sensor impulse shape. More will be said about amplitude versus area in the Discussion section.

4. Digital Signal Processing Section

The signal processing section consists of multiple processing blocks, some of which are optional.

4.1. Goertzel Algorithm

As shown in Figure 6, the top left is the disdrometer sensor. The analog signal is mixed with a tone pulse triggered by the tipping bucket. The tone pulse width is very short compared to the time between tips and therefore does not degrade the drop spectra measurement. The Goertzel decoder separates the tip tones from the sensor signal and creates a list of tip times. The *tip times list*, $\{t_k\}$, yields rainfall rate. The band pass filter section consists of optional filtering stages implemented as user selectable order low pass and high pass filters. Different processing strategies determine the cut-off frequencies of these filters relative to the resonant frequency of

the sensor. The resonant frequency of the sensor is mostly determined by the encapsulant properties, primarily hardness.

4.2. Peak Detector

The next section is the peak detector. This section creates a list of peak amplitudes versus time, $\{x_n, t_n\}$, for all drops measured. The number of impulses per second can easily range from 1 to 50 depending on rainfall rate and type of rainfall. The total number of drops, or drop flux, is proportional to the area of the sensor. The drop impulse width, as shown in Figure 5, is dependent on the sensor characteristics, and again is mostly determined by the encapsulant material properties. A typical impulse width is dependent on the drop size, and for the largest drops (5-6 mm), 30 ms might be required for the impulse to fall below a noise threshold. For extreme rainfall rates, the flux may exceed 30 drops per second and as one can see, the trade-off between sensor size and coincidence of drop impulses sets the size of the sensor area to something in the 50 cm^2 range. The biggest challenge of the peak detector is to not miss an impulse, while at the same time, not counting false impulse from a decaying large drop, splashing from large drops can also lead to false counts. All of these issues are addressed, at least in part, by an adaptive dead time strategy after a peak is detected and measured.

4.3. Image Spot Processing

The laser/camera system is triggered by the tipping bucket for convenience. This is not a requirement, but does result in a simpler processing methodology. The video camera images are converted to a spot and an average greyscale value is determined, corresponding to the tip time. For the 5mW, 532 nm green laser used in this work, the green component of the image is most sensitive to the laser, whereas the red and blue components are good indicators of background noise.

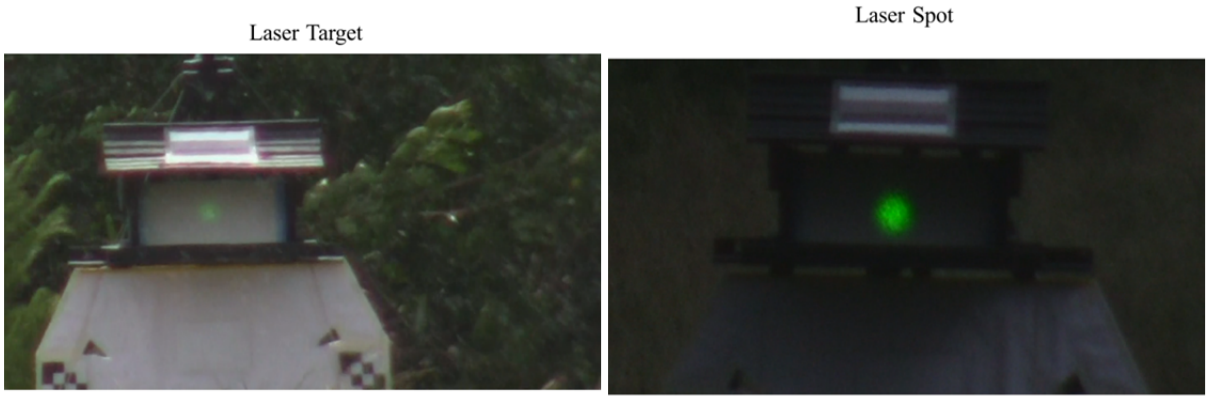

The algorithm used to convert the RGB color to greyscale intensity, which can then be converted to extinction coefficient, is shown below. The filtered value is averaged over the spot within a half intensity diameter. The diameter of the spot is also recorded, but only the intensity data is used in the final calibration. Other details of the laser measurement, including optimal distance, are discussed in (Lane, 2013).

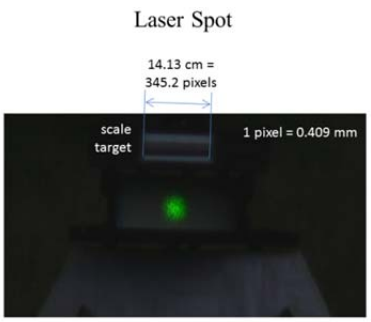

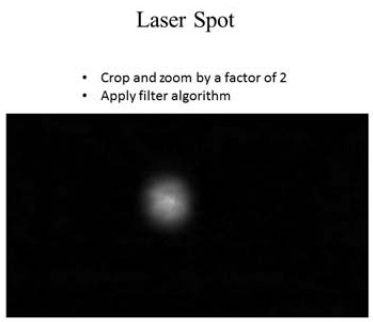

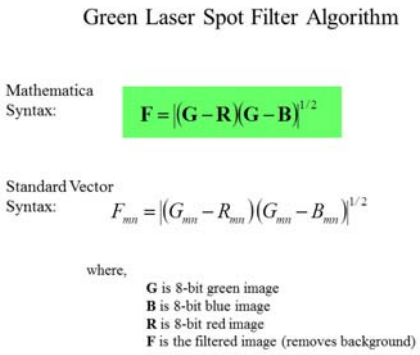

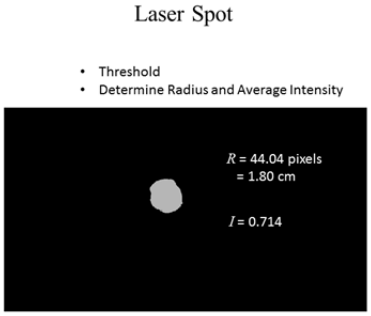

4.4. Calibration Algorithm

The calibration processing technique is an extension of that described in (Kasparis, 2010). The current method is formulated in the same way as (Kasparis, 2010), but an additional term is included in the error minimization. In the equations below, the **A** matrix corresponds to the tipping bucket data, while the **B** matrix is due to the optical extinction data. The calibration parameter vector **P** contains two sets of coefficients, α and β. The sub-vector α is equivalent to the calibrations vector **P** in (Kasparis, 2010). This approach is not the only way to set the problem up, but it is a convenient method in that two sets of independent calibration curves are created, one from the tipping bucket data, and one from the laser/camera data. By forcing the two sets to converge is one simple strategy to generating a acceptable calibration. A final calibration, after the two sets of curves have r converged, is just the geometric mean of the two.

*** The following will be converted to Word, but for purposes of the DAA review draft, it will remain as a PowerPoint insert (the conversion will be a format change only):

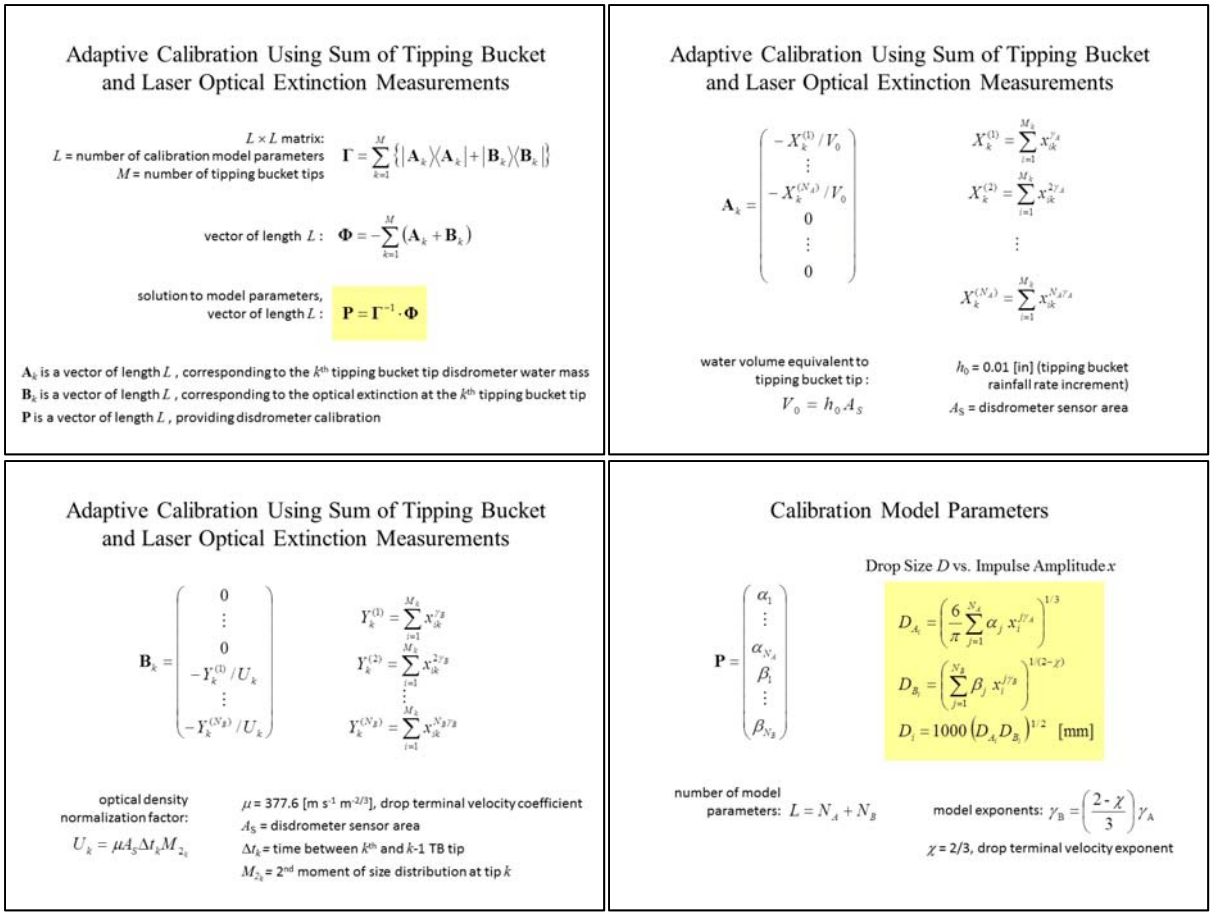

5. Example Data Processing

On August 8, 2013, between 21:00 and 22:30 UTC (5:00 PM and 6:30 PM local time), data was collected at a site 17 km, 323.7° from the KLMB radar. Figure 7 shows the equipment setup. Tipping buckets, accumulation gauge, UCF-DHD, and laser target are set up outside of the research vehicle. All electronics, including green laser, video camera, processing electronics, and audio recorder (for disdrometer), are inside of the vehicle and powered by the vehicle's 12 V battery. The laser and camera are aligned so that the partially opened window does not interfere with the laser light beam. The vehicle and target are aligned to the approach of the oncoming storm so that the wind is generally opposite the partially opened window, thus minimizing the problem of rain damaging the electronics, laser, and camera. The equipment setup is shown in Figure 7, where the top left shows a tipping bucket, accumulation gauge, and laser target, barely visible in background. The bottom left of Figure 7 shows the laser and camera set up, with all electronics, inside of a vehicle, powered by car battery. The right portion of Figure 7 shows through the vehicle window, tipping buckets, rain gauge, and UCF-DHD.

Figure 8 is the result of processing the laser /camera data. The green lines represent the normalized laser intensity viewed by the video camera on the target, where the round trip distance $2L$ = 150 m, and each vertical line corresponds to a rain gauge bucket tip. The blue lines at the bottom of Figure 8 are estimates of the back scatter from the rain, which increases with increased rainfall rate. This background is subtracted from the intensity (green lines), then

converted to extinction coefficient, α, shown by the black line. In Figure 9, both the tipping bucket and optical extinction calibration curves are overlaid, but have converged to appear as one curve.

Figure 10 shows the results of the calibration, where drop spectra is plotted as black dots. The green lines are optical density, where the thin line is from the laser measurement, while the thick line is derived from the computed DSD. The blue lines are rainfall rate, where the thin line is from the tipping bucket measurement, while the thick line is derived from the computed DSD. Finally the black lines are the computed radar reflectivity, where the thin line derived from the laser measurement and assumption of a pure exponential DSD model, whereas the think line is derived from the DSD.

The NEXRAD reflectivity did not track the reflectivity well. However, since the disdrometer derived reflectivity is consistent with the reflectivity computed from the exponential DSD model with parameters determined from a fit to the rainfall rate and optical density, the NEXRAD reflectivity becomes suspect. It has been suggested that this type of disagreement between NEXRAD reflectivity and disdrometer reflectivity can be resolved by a simplistic approach, based on the assumption of a constant vertical velocity (updraft or downdraft) occurring during the course of the measurement (Ahammad, 2002). In this case, a down draft velocity can explain most of the NEXRAD reflectivity discrepancy.

6. Discussion

A disdrometer calibration method has been described, based on a collocated measurement of laser extinction. Laser extinction due to rainfall is proportional to the second moment of the drop size distribution as measured by the disdrometer. This equivalence provides an opportunity to form a least squares error minimization. Since previous work took the same approach using a collocated tipping bucket, the method investigated in this paper uses both a tipping bucket and laser extinction to form the error function to be minimized. The result is two calibration curves, one from the tipping bucket data, and one from the laser extinction. By adjusting parameters so that both calibration curves converge, a higher confidence in the final calibration results.

7. References

Ahammad, Parvez, Christopher R. Williams, Takis Kasparis, John Lane, Francis Merceret, and Linwood Jones. "Vertical air motion estimates from the disdrometer flux conservation model and related experimental observations." In*AeroSense 2002*, pp. 384-393. International Society for Optics and Photonics, 2002.

Kasparis, Takis, John Lane, and Linwood Jones. "Modeling of an impact transducer for in situ adaptive disdrometer calibration." In *Communications, Control and Signal Processing (ISCCSP), 2010 4th International Symposium on*, pp. 1-4. IEEE, 2010.

Lane, John E., Linwood Jones, Takis C. Kasparis, and Philip Metzger. "Measurements of DSD Second Moment Based on Laser Extinction." (2013).

Lane, John E., Takis Kasparis, Philip T. Metzger, and W. Linwood Jones. "Spatial and Temporal Extrapolation of Disdrometer Size Distributions Based on a Lagrangian Trajectory Model of Falling Rain." *arXiv preprint arXiv:0906.1614*(2009).

Fig. 1. (Color online) Top: Roof of UCF Engineering Building, showing three tipping bucket rain gauges (white cylinders) and three disdrometers: Joss disdrometer on left, and two UCF-DHD disdrometers in center and far right. Bottom: CUT-DHD on the roof of the Cyprus University of Technology.

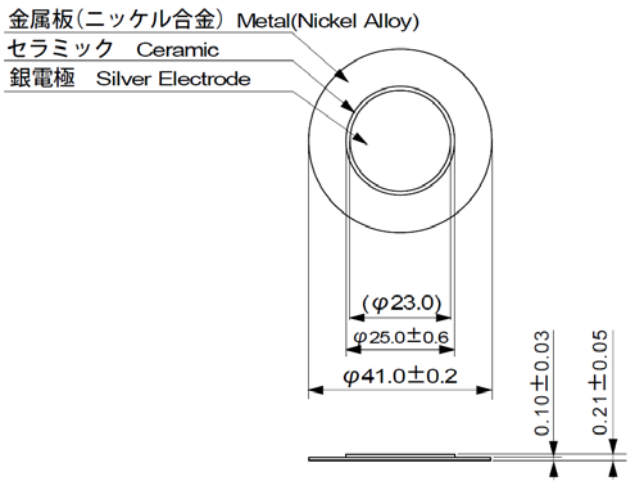

Fig. 2. Dimensions of muRata 7NB-41-1 piezoelectric diaphragm (dimensions in mm).

Fig. 3. (Color online) Multi-ceramic sensor fabrication – total sensor area equal to 65 cm^2. Left: intermediate stage of fabrication showing ceramic and wiring in mold before adding epoxy. Right: Complete units before final mounting.

Fig. 4. (Color online) Dual head disdrometer design using largest available COTS piezoelectric disk, the muRata 7NB-41-1. Left: UCF prototype; Right: refined CUT version.

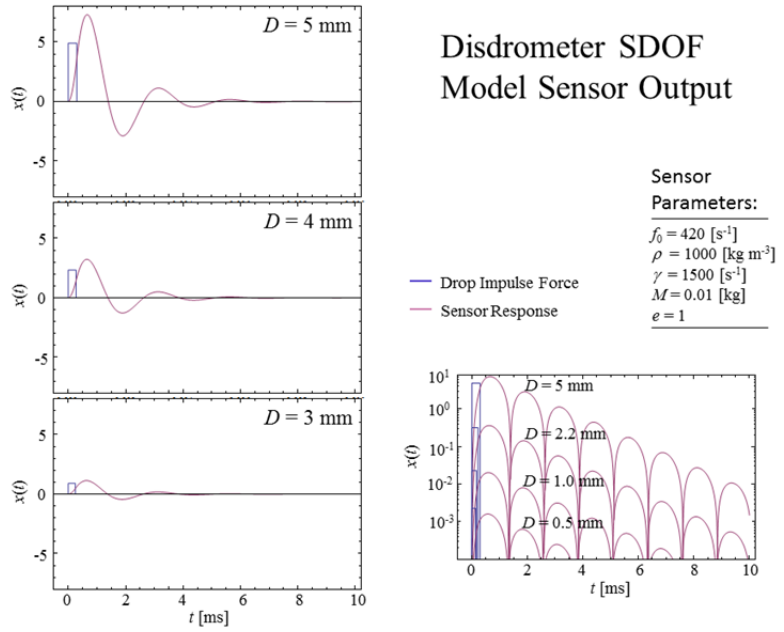

Fig. 5. (Color online) SDOF output using typical sensor values.

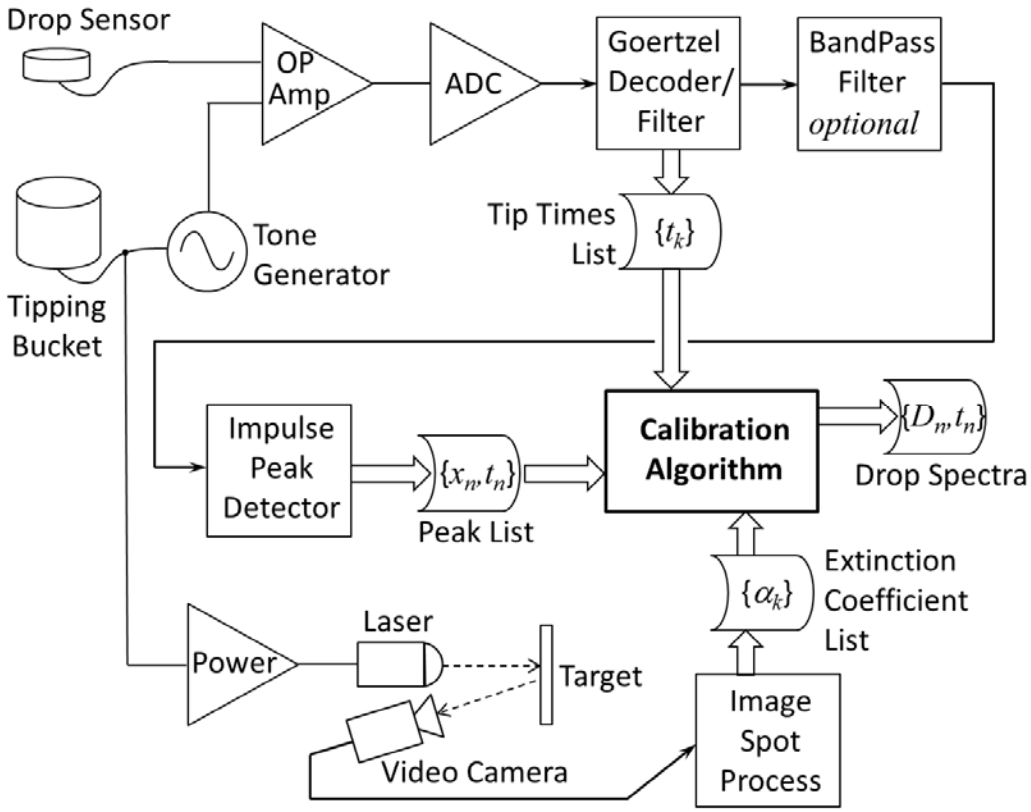

Fig. 6. Block diagram of system signal processing.

Fig. 7. Equipment setup: Top left: tipping bucket, accumulation gauge and laser target barely visible in background; Bottom left: laser and camera set up with all electronics inside of a vehicle, powered by car battery; Right: tipping buckets, rain gauge, and UCF-DHD shown through vehicle window.

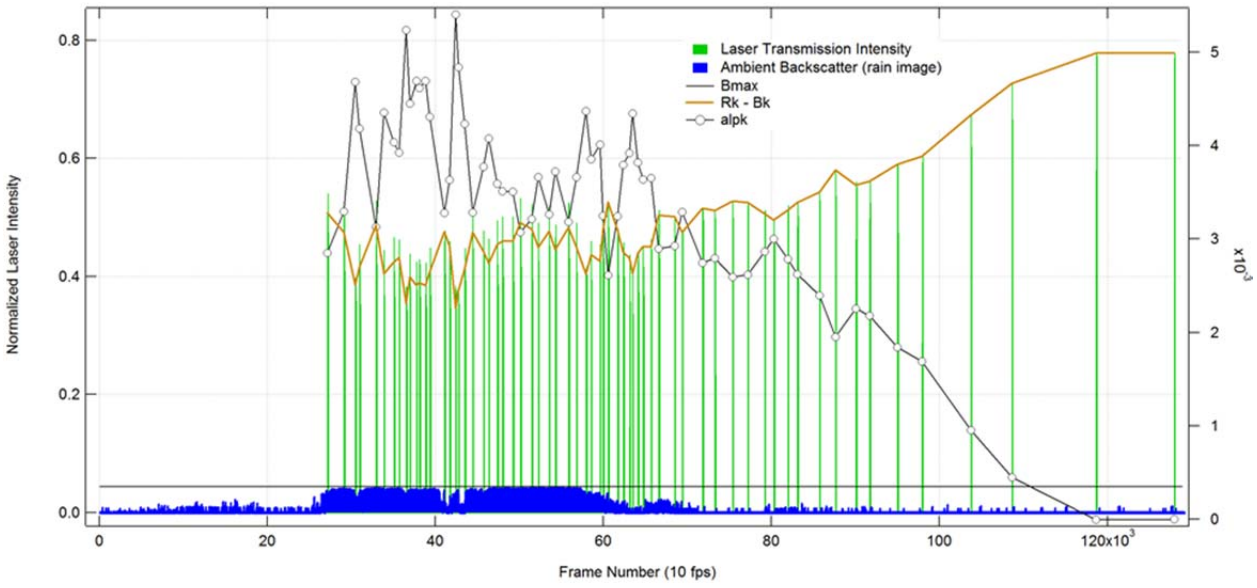

Fig. 8. Green lines represent the normalized laser intensity viewed by the video camera on the target, where the round trip distance $2L$ = 150 m, and each vertical line corresponds to a rain gauge bucket tip. The blue lines at the bottom are estimates of the back scatter from the rain, which increases with increased rainfall rate. This background is subtracted from the intensity (green lines), then converted to extinction coefficient, α, shown by the black line.

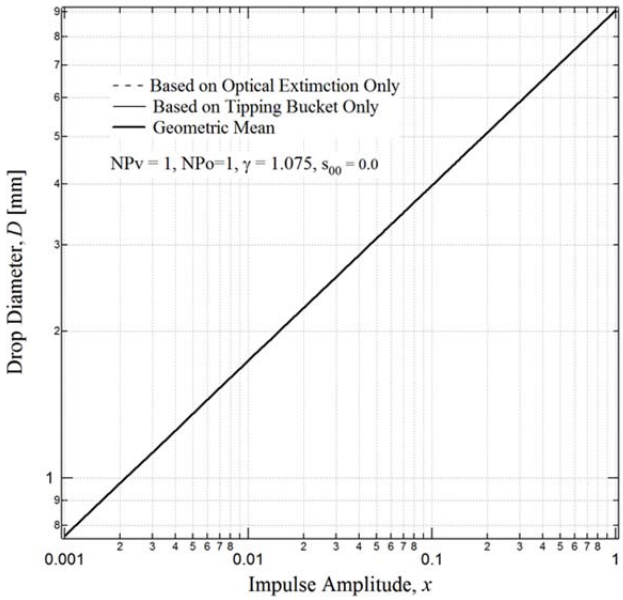

Fig. 9. Both the tipping bucket and optical extinction calibration curves are overlaid, but have converged to appear as one curve.

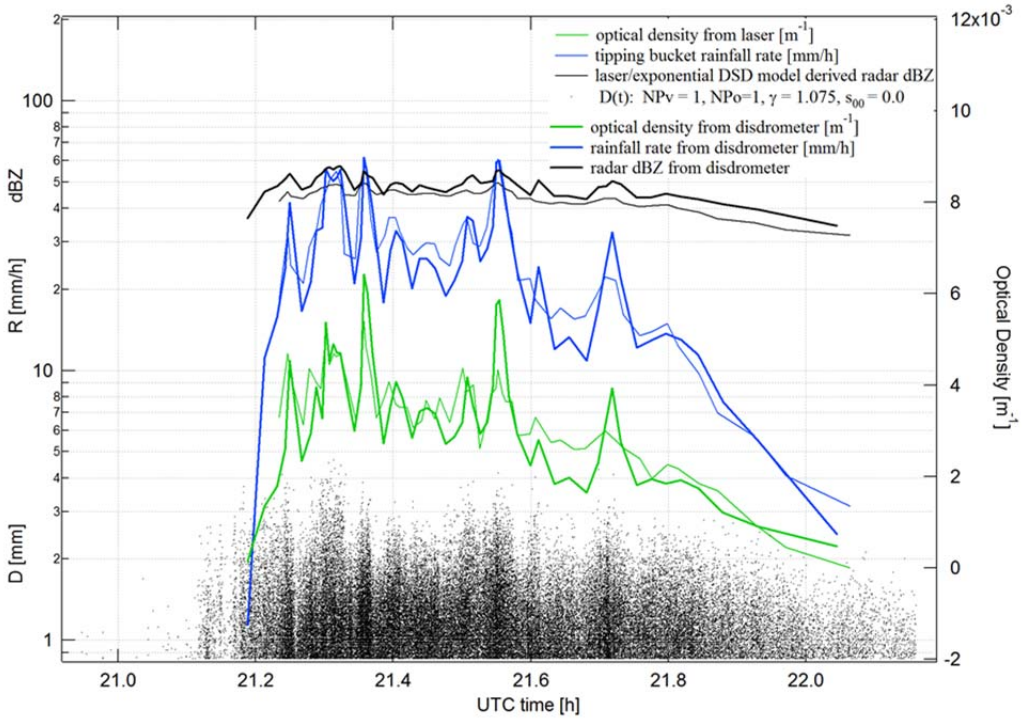

Fig. 10. Drop spectrum is plotted as black dots. The green lines are optical density, where the thin line is from the laser measurement, while the thick line is derived from the computed DSD. The blue lines are rainfall rate, where the thin line is from the tipping bucket measurement, while the thick line is derived from the computed DSD. The black lines are the computed radar reflectivity, where the thin line derived from the laser measurement and assumption of a pure exponential DSD model, whereas the think line is derived from the DSD.